Article

# Near-to-Far Field Transformations for Radiative and Guided Waves

Jianji Yang,*[†,#] Jean-Paul Hugonin,*[‡] and Philippe Lalanne*[†]

[†]Laboratoire Photonique Numérique et Nanosciences (LP2N, UMR 5298), Institut d'Optique d'Aquitaine, CNRS−IOGS−Université Bordeaux, 33400 Talence, France
[‡]Laboratoire Charles Fabry (LCF, UMR 8501), CNRS−IOGS−Université Paris-Sud, 2 Avenue Augustin Fresnel, 91127 Palaiseau, France

Ⓢ Supporting Information

ABSTRACT: Light emitters or scatterers embedded in stratified media may couple energy to both free-space modes and guided modes of the stratified structure. For a comprehensive analysis, it is important to evaluate the angular intensity distribution of both the free-space modes and guided modes excited in such systems. In the present work, we propose an original method based on Lorentz reciprocity theorem to efficiently calculate the free-space and guided radiation diagrams with a high accuracy from the sole knowledge of the near-field around the emitters or scatterers. Compared to conventional near-to-far field transformation techniques, the proposal allows one to easily evaluate the guided-mode radiation diagrams, even if material dissipation is present in the stack, and thus to simultaneously track the coupling of light to all channels (i.e., free-space and guided ones). We also provide an open-source code that may be used with essentially any Maxwell's equation solver. The numerical tool may help to engineer various devices, such as light-emitting diodes or nanoantennas, to achieve directional and efficient radiative spontaneous decays in free-space and guided optics.

KEYWORDS: light emission, light scattering, mode expansion, radiation diagram, stratified structure, Lorentz reciprocity, computational electrodynamics
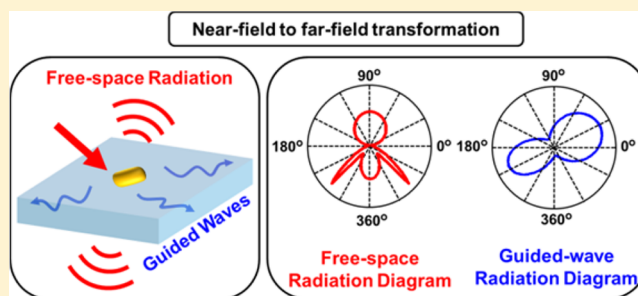
W hen excited either by propagative electromagnetic waves (e.g., plane waves or guided waves) or by local sources such as dipole emitters, individual scatterers or aggregates of scatterers embedded in a stratified medium may couple light into multiple channels including guided modes of the stratified structure and free-space radiative modes of the claddings. The coupling mechanism plays a central role in a large variety of research topics in photonics, for instance, for improving the performance of thin-film solar cells using metal nanoparticles,[1,2] enhancing light extraction in light-emitting devices using nanoparticles,[3−5] achieving directional light scattering[6,7] or emission[8−10] using nanoantennas,[11] realizing various optical functionalities (e.g., beam steering[12,13] and shaping[14]) with metasurfaces based on nanoresonator arrays, or engineering the scattering properties of plasmonic nano-objects such as metallic slits/grooves[15−17] and metallic holes.[18−20]

In electromagnetic simulations with Maxwell's equation solvers, usually one can easily compute only the near-zone field around the scatterers. However, the far-zone field is often of great interest because it contains all the information on the so-called *free-space radiation diagram*, which describes the angular distribution of the energy flux density radiated into free space, and the *guided-mode radiation diagram*, which describes the angular distribution intensity radiated into guided modes of the stratified medium. Numerical techniques capable of computing far-zone radiation diagrams only using near-zone field distributions are usually referred to as near-to-far field transformation (NFFT) approaches. The latter are mature techniques in microwave engineering.[21] Nearly all numerical implementations of NFFT techniques rely on the field equivalence principle (or Huygens' principle),[21] which allows us to replace the radiated field of an antenna in the near-field zone by equivalent current sources and then to generate far-zone fields using the free-space Green's function and the equivalent sources. For antennas placed in a stratified substrate, the free-space Green's function must be replaced by Green's functions that account for the strata.[22,23]

Many authors have contributed to the elaboration of numerical methods on NFFT approaches, in various fields of physics, maybe starting from initial works on the emission and propagation of radio waves above the earth.[24] However, it appears that the literature contains only scattered electromagnetic contributions and that a unified numerical tool that retrieves both free-space and guided-mode radiation diagrams is still lacking, at least in the optical domain.[23] Hereafter, we remove this deficiency and establish a formalism to retrieve the far-zone field from the near-zone field for electromagnetism problems due to the scattering by *local inhomogeneities* in

stratified media. We also provide an open-source NFFT toolbox,[25] which retrieves the far-field radiation diagrams from the knowledge of the permittivities and permeabilities of the layers (assumed uniform and isotropic) of the stratified structure and of the near-zone field that can be obtained with virtually any Maxwell's equation solver on a closed surface surrounding the local inhomogeneity.

To be more precise, let us consider a planar stratified medium, in which a few scatterers are embedded (see Figure 1a). We further consider a parallelepipedic box that fully
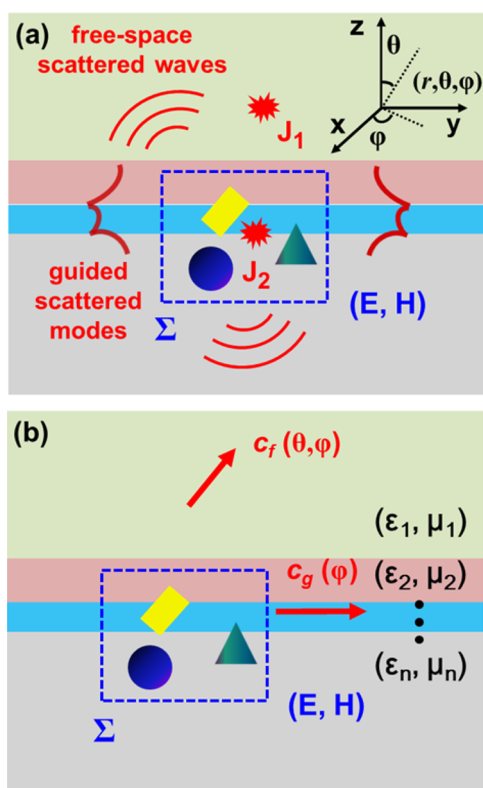

Figure 1. Radiation diagram calculation due to the scattering of local inhomogeneities in a stratified medium. (a) The scatterers (rectangle, sphere, and triangle) may be excited by either a far-field source J_1 or a near-field source J_2. They excite both free-space radiative modes and guided modes of the stratified structure. (b) Retrieval of the angular distribution of plane-wave amplitudes $c_f(\theta, \varphi)$ and guided-mode amplitudes $c_g(\varphi)$. The blue closed "box" Σ fully encloses all the *local inhomogeneity*, so that the geometry outside the box should be the stratified medium. The retrieval of $c_f(\theta, \varphi)$ and $c_g(\varphi)$ requires the knowledge of the field $(\mathbf{E,H})$ on the "box", the relative permittivity, and permeability of every layer. In practice, a small-sized box can be used and $(\mathbf{E,H})$ on the box can be obtained with any Maxwell's equation solver. The accompanying open-source code performs rapid computation of the radiation diagrams (amplitude and intensity) of the free-space radiated waves and the guided waves. Inset in (a) shows the coordinates.

encloses the scatterers, so that the geometry outside the box is strictly the stratified medium without any inhomogeneity. The blue closed "box" Σ of Figure 1a provides an example. The inhomogeneities might be illuminated by an external source, such as J_1 in Figure 1a, which is placed outside the box (if the source is very far, then the illumination is a plane wave) or by a localized source, such as J_2 in Figure 1a, which is placed inside the box. We assume that with some Maxwell's equation solver

one is able to calculate the electromagnetic field $(\mathbf{E,H})$ on the box. $(\mathbf{E,H})$ can be either

- for $J_2 = 0$, the scattered field induced by the inhomogeneities and obtained as the difference between the total field and the background field (which is generated by the source J_1 illuminating the stratified medium in the absence of the inhomogeneities);
- for $J_1 = 0$, the total field generated by the source J_2 that illuminates the embedded scatterers (this situation represents a typical extraction problem encountered with light-emitting devices);
- any linear combination of the two previous cases.

For all cases, $(\mathbf{E,H})$ on the box is formed only by outgoing (regarding the "box") plane waves and outgoing guided modes (no incoming fields), and the present NFFT method and open-source toolbox may accurately retrieve the far-field radiation diagrams for guided and free-space modes from the sole knowledge of $(\mathbf{E,H})$ and the permittivities and permeabilities of the layers (assumed uniform and isotropic) of the stratified structure. The approach is very general, as it applies to inhomogeneities with arbitrary shapes, any materials, and any thin-film stack, even for lossy dielectric or metallic materials. The only requirement is that all material must be reciprocal, i.e., $\varepsilon = \varepsilon^T$ and $\mu = \mu^T$, where the superscript "T" denotes the transpose operator.

This article is organized as follows. First, we briefly describe a general NFFT method for calculating the free-space radiation diagrams. Then, as the main contribution of the present work, the formulation of a novel and substantially analytical method to retrieve guided-mode radiation diagrams is proposed. Third, the efficiency and applicability of the numerical tool is exemplified by studying some basic light scattering/emission problems in stratified media, and the validity and accuracy of the open-source code is tested. In the last section, the usage of the open-source tool and the conditions under which the tool may be used safely are summarized.

■ A CLASSICAL APPROACH TO RETRIEVE THE FREE-SPACE RADIATION DIAGRAMS

In this section, we describe an NFFT method to retrieve the far-zone free-space radiation diagrams. This is a classical problem in electromagnetism, which has already been treated by many authors; see for instance the recent works in refs 22 and 23 based on a Green's dyadics approach and the field equivalence principle. A largely equivalent approach based on Lorentz reciprocity theorem is briefly outlined hereafter. This is not the main focus of the present work; however, we think it is still worth being documented concisely for the sake of completeness, since it is implemented in the open-source NFFT tool and is inherently linked to the original contribution, the NFFT of guided modes, which is presented in the next section.

We consider the radiation diagram into the upper half-space ($z \to \infty$) of the field distribution $(\mathbf{E,H})$, assuming $\mathrm{Im}(\varepsilon_1) = 0$ and $\mathrm{Im}(\mu_1) = 0$. The radiation in the lower half-space is treated similarly. Since the radiation diagram essentially describes the angular distribution of the energy flux density, the retrieval consists in performing a plane-wave decomposition of $(\mathbf{E,H})$ and to compute the amplitudes of the radiated plane waves for every direction. Both TE- and TM-polarized waves have to be taken into account for every direction, as implemented in the open-source code; however, because plane waves with

orthogonal polarizations are independently retrieved, in the following we consider purely TE- or TM-polarized waves to reduce cumbersome notations.

It is convenient to first consider the upward-going plane wave (either TE- or TM-polarized) that propagates away from the scatterers in the directions defined by (θ, φ); see the inset in Figure 1a. The plane wave is denoted by $(\hat{E}_0^+, \hat{H}_0^+) \exp[i(ux + vy + \chi z)]$, with the superscript "+" of $\hat{E}_0^+$ and $\hat{H}_0^+$ labeling upward-going waves (a minus sign is used hereafter for downward-going waves), and $u = k_0\sqrt{\varepsilon_1\mu_1} \sin(\theta) \cos(\varphi)$, $v = k_0\sqrt{\varepsilon_1\mu_1} \sin(\theta) \sin(\varphi)$, and $\chi = k_0\sqrt{\varepsilon_1\mu_1} \cos(\theta)$, with k_0 denoting the wavenumber in a vacuum. In an horizontal plane at $z = z_1$ in the upper half-space, $(\mathbf{E}, \mathbf{H})$ can be expanded as

$$\mathbf{E}(x, y, z_1) = \iint c_f^+(\theta, \varphi)\hat{E}_0^+ \exp[i(ux + vy + \chi z_1)] \, du$$
$$dv \tag{1.1}$$

$$\mathbf{H}(x, y, z_1) = \iint c_f^+(\theta, \varphi)\hat{H}_0^+ \exp[i(ux + vy + \chi z_1)] \, du$$
$$dv \tag{1.2}$$

where $c_f^+(\theta, \varphi)$ denotes the plane-wave amplitude coefficient. In principle, $c_f^+(\theta, \varphi)$ can be found with inverse Fourier transform. However, this requires the knowledge of the radiated field in the entire (infinite) plane $z = z_1$, which is not suitable for numerical calculations.

Indeed, according to Lorentz reciprocity theorem, $c_f^+(\theta, \varphi)$ can be obtained by computing a surface integral on a closed "box" Σ surrounding the local inhomogeneities (see Figure 1b):

$$c_f^+(\theta, \varphi) = \frac{k_0 Z_0 \mu_1}{8\pi^2 \chi \hat{E}_0^+ \cdot \hat{E}_0^-} \oint_\Sigma (\mathbf{E} \times \hat{H}^- - \hat{E}^- \times \mathbf{H}) \, d\mathbf{S} \tag{2}$$

where Z_0 denotes the vacuum impedance and $(\hat{E}^-, \hat{H}^-)$ represents the field that is created by a downward plane wave $(\hat{E}_0^-, \hat{H}_0^-)\exp[-i(ux + vy + \chi z)]$ impinging onto the stratified medium (without the inhomogeneities). The flux density at direction (θ, φ) can be found as $\frac{1}{2}\sqrt{\varepsilon_0\varepsilon_1/(\mu_0\mu_1)} |c_f^+(\theta, \varphi)|^2 |\hat{E}_0^+|^2$. In passing, we emphasize that, because the vectorial field $(\hat{E}^-, \hat{H}^-)$ induced by a plane wave in a stratified structure can be calculated rather easily with 2×2 matrix products for every incidence and polarization,[22,26] the overlap integral of eq 2 can be computed in parallel for all directions and the $c_f^+(\theta, \varphi)$ coefficients can be computed very efficiently (see Technical Remarks).

We do not provide a demonstration of eq 2 with the Lorentz reciprocity theorem hereafter; it is technical and essentially echoes the classical NFFT techniques based on the field equivalence principle,[21] without explicitly considering the equivalent current sources.

■ SEMIANALYTICAL APPROACH TO RETRIEVE THE GUIDED-MODE RADIATION DIAGRAMS

In this section, an original NFFT approach for retrieving guided-mode radiation diagrams for planar stratified structure is formulated. We again consider the emission problem sketched in Figure 1b, in which the guided modes of the planar stratified

structure may be launched in all in-plane directions [i.e., $0 < \varphi < 2\pi$].

Before going to details, we would like to briefly address the following question: bearing in mind the NFFT method for free-space waves described in the former section, can we extract the guided-mode radiation diagram by performing, similarly to eq 2, an overlap integral on the closed "box" Σ between the field $(\mathbf{E}, \mathbf{H})$ and the field of the associated incident guided mode propagating in the direction φ, i.e., replacing the incident plane wave $(\hat{E}^-, \hat{H}^-)$ by an incident guided mode with an in-plane wavevector parallel to the azimuthal direction φ? The answer that can be easily derived from the Lorentz reciprocity theorem is yes for nonlossy materials, but the treatment is problematic for lossy modes because one needs to handle exponentially large fields.

To remove this difficulty, we formulate a novel and substantially analytical approach that allows one to evaluate the radiation diagram of guided modes with a high accuracy, for lossy (dielectric or metallic) stratified structures. The method requires only the knowledge of the field $(\mathbf{E}, \mathbf{H})$ on the closed box Σ and of the guided-mode profile. All the derivation steps are provided hereafter, with some technical details being documented in the SI.

Cylindrical Waveguide Modes. We start by expanding the radiated field $(\mathbf{E}, \mathbf{H})$ using waveguide modes of the stratified structure defined in a cylindrical coordinate system (r, φ, z); see Figure 2. When solving source-free Maxwell's equations
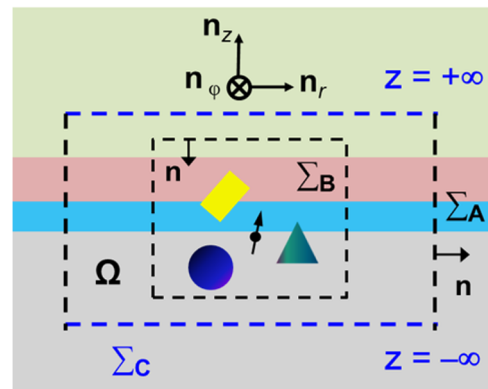

Figure 2. Domain Ω with its boundaries. Σ_A (vertical black dashed lines) defines a cylindrical surface of radius r that extends from $z = -\infty$ to $+\infty$, Σ_B is a closed "box" that encloses the inhomogeneity, and Σ_C corresponds to the upper and lower horizontal surfaces (blue dashed lines) of the cylinder at $|z| = \infty$. Σ_A and Σ_C together form the outer boundary of the volume Ω, and Σ_B is the inner boundary. The outward surface normal of Ω is denoted by $\mathbf{n}$.

(eigenmode problems) of stratified planar waveguides, the eigenmodes can be written as the product of functions with separated variables, z, φ, and r, with the r-dependent part expressed with Hankel functions (see SI). Hereafter, the mth-order TE- or TM-polarized modes with propagation constants k_m will be denoted as $\Phi_{+m,n} = (\hat{E}_{m,n}^+ \exp(in\varphi), \hat{H}_{m,n}^+ \exp(in\varphi))$ for outgoing (to $r \to \infty$) modes propagating and $\Phi_{-m,n} = (\hat{E}_{m,n}^- \exp(-in\varphi), \hat{H}_{m,n}^- \exp(-in\varphi))$ for ingoing (to $r \to 0$) modes, with n ($n = 0, \pm1, ...$) determining the azimuthal pattern and $(\hat{E}_{m,n}^\pm, \hat{H}_{m,n}^\pm)$ describing the r- and z-dependent profiles. Note that due to the separation of variables r and φ, for a given polarization, each order m embraces a series of

azimuthal harmonics with the same propagation constant k_m but with different azimuthal pattern determined by $\exp(\pm in\varphi)$. The explicit expressions of mode profiles (including both the general expression and asymptotic expression at $r \rightarrow \infty$) are provided in the SI for TE and TM modes.

Mode Expansion. As in the previous section, we assume that the modes are either TE- or TM-polarized. The total electric field **E** can be decomposed into a set of outgoing guided cylindrical modes and a continuum of radiation modes:

$$\mathbf{E}(r, \varphi, z) = \sum_m \sum_n c_{m,n}^+ \hat{E}_{m,n}^+(k_m r, z) \exp(in\varphi)$$

$$+ \text{ continuum} \qquad (3)$$

where $c_{m,n}^+$ denotes the amplitude of the nth *azimuthal harmonic* of the mth outgoing mode for the polarization considered. The second term, "continuum", in eq 3 corresponds to a summation over the continuum of radiation modes of the stratified waveguide; we provide some additional discussions in the SI about the orthogonality and normalization of radiation modes.

Asymptotic Behavior and Radiation Diagram. The electric field of the mth outgoing mode can be expressed as a summation of all the relevant azimuthal harmonics, i.e., $\mathbf{E}_m(r, \varphi, z) = \sum_{n=-\infty}^{+\infty} c_{m,n}^+ \hat{E}_{m,n}^+(k_m r, z) \exp(in\varphi)$. The asymptotic behavior at $r \rightarrow \infty$ can be found with asymptotic forms of Hankel functions, and for a TM mode, for instance, we have

$$\mathbf{E}_m(r \rightarrow \infty, \varphi, z)$$

$$= f_m(\varphi) \exp(ik_m r)/\sqrt{r} \, [e_{\mathrm{L}}(z)\mathbf{n}_r, \, 0\mathbf{n}_\varphi, \, e_{\mathrm{T}}(z)\mathbf{n}_z] \qquad (4)$$

where $f_m(\varphi) = \sum_{n=-\infty}^{+\infty} c_{m,n}^+ \exp[-i(2n+1)\pi/4]\sqrt{2/(\pi k_m)}$

$$\exp(in\varphi)$$

describes the angular distribution of the amplitude of the mth mode in the far zone and $e_{\mathrm{L}}(z)$ and $e_{\mathrm{T}}(z)$ represent the longitudinal and transverse electric field components of the z-dependent mode profile (see SI). $|f_m(\varphi)|^2$ characterizes the angular intensity distribution in the far zone, i.e., the *guided-mode radiation diagram*.

If the stack materials are lossless, the total power carried by the mth mode can be found by summing the power of all azimuthal harmonics as $P_m = \int_0^{2\pi} |f_m(\varphi)|^2 \, d\varphi = 4/|k_m| \sum_{n=-\infty}^{+\infty} |c_{m,n}^+|^2$, provided that the modes are normalized in such a way as $N_{m,n} = (-1)^n \, 16/k_m$, with $N_{m,n}$ denoting the normalization coefficient of $\Phi_{\pm m,n}$ defined as (see SI)

$$N_{m,n} = \int_0^{2\pi} d\varphi \int_{-\infty}^{+\infty} (\hat{E}_{m,n}^+ \times \hat{H}_{m,n}^- - \hat{E}_{m,n}^- \times \hat{H}_{m,n}^+) \cdot \mathbf{n}_{\mathrm{r}} r$$

$$dz \qquad (5)$$

The integral in eq 5 runs over a vertical cylindrical surface of radius r with an infinite transverse cross-section from $z = -\infty$ to $z = +\infty$ (e.g., surface Σ_{A} in Figure 2), and noticeably it involves both the ingoing and the outgoing modes. It is independent of r even in the presence of absorption. A similar normalization approach for guided modes can be found in ref 27.

Calculation of the Mode Amplitude. Here we will demonstrate that the amplitude coefficient $c_{m,n}^+$ of the mode $\Phi_{+m,n}$ in eq 3 can be found with a simple overlap integral [see eq 11] involving (**E**,**H**) and the ingoing mode $\Phi_{-m,n}$ on the closed "box" Σ_{B} defined in Figure 2.

For that, we define the inner product between two modes $\Phi_{\sigma m,n} = (\hat{E}_{m,n}^\sigma \exp(\sigma in\varphi), \hat{H}_{m,n}^\sigma \exp(\sigma in\varphi))$ a n d $\Phi_{\xi p,q} = (\hat{E}_{p,q}^\xi \exp(\xi iq\varphi), \hat{H}_{p,q}^\xi \exp(\xi iq\varphi))$ (here we use σ and ξ to label the propagation direction, i.e., $\sigma = \pm 1$ and $\xi = \pm 1$) as

$$\Phi_{\sigma m,n} \otimes \Phi_{\xi p,q} = \int_0^{2\pi} \exp[i\varphi(\sigma n + \xi q)]$$

$$d\varphi \times \int_{-\infty}^{+\infty} (\hat{E}_{m,n}^\sigma \times \hat{H}_{p,q}^\xi - \hat{E}_{p,q}^\xi \times \hat{H}_{m,n}^\sigma) \cdot$$

$$\mathbf{n}_r r \, dz \qquad (6)$$

where $\otimes$ denotes the inner product operator. Equation 6 is also defined for a vertical infinite cylindrical surface, as for eq 5. On the basis of the Lorentz reciprocity theorem, we establish the unconjugated form of mode orthogonality relation (see SI)

$$\Phi_{\sigma m,n} \otimes \Phi_{\xi p,q} = \delta_{\sigma m, -\xi p} \delta_{n,q} N_{m,n} \quad (\sigma = \pm 1, \, \xi = \pm 1) \qquad (7)$$

From eq 3 by using the orthogonality relation of eq 7, we find

$$c_{m,n}^+ = (\mathbf{E}, \mathbf{H}) \otimes \Phi_{-m,n}$$

$$= \frac{1}{N_{m,n}} \int_0^{2\pi} \exp(-in\varphi) \, d\varphi$$

$$\int_{-\infty}^{+\infty} (\mathbf{E} \times \hat{H}_{m,n}^- - \hat{E}_{m,n}^- \times \mathbf{H}) \cdot \mathbf{n}_r r \, dz \qquad (8)$$

As the orthogonality and normalization relations are both r-independent (see SI), eq 8 is r-independent as long as the cylindrical surface, such as Σ_{A} shown in Figure 2, fully surrounds the inhomogeneity.

Nevertheless, eq 8 is not suitable for numerical implementation, since it requires an integral over the entire transverse direction, $-\infty < z < +\infty$. Thus, we consider a closed *source-free* volume Ω with its boundary Σ formed by three surfaces, Σ_{A}, Σ_{B}, and Σ_{C}; see Figure 2. Applying (**E**,**H**) and $\Phi_{-m,n}$ to the Lorentz reciprocity theorem (see SI or ref 27) for the volume Ω, a simple but vital relation can be found as $\oint_\Sigma \exp(-in\varphi)(\mathbf{E} \times \hat{H}_{m,n}^- - \hat{E}_{m,n}^- \times \mathbf{H}) \cdot \mathbf{n} \, dS = 0$, owing to the fact that (**E**,**H**) and $\Phi_{-m,n}$ share the same permittivity and permeability distribution in Ω. Furthermore, as we consider the mth mode to be a bound mode with a field that exponentially vanishes at $z = \pm\infty$,

$$\oint_{\Sigma c} \exp(-in\varphi)(\mathbf{E} \times \hat{H}_{m,n}^- - \hat{E}_{m,n}^- \times \mathbf{H}) \cdot \mathbf{n} \, dS = 0 \qquad (9)$$

and we get

$$\int_{\Sigma_{\mathrm{A}}} \exp(-in\varphi)(\mathbf{E} \times \hat{H}_{m,n}^- - \hat{E}_{m,n}^- \times \mathbf{H}) \cdot \mathbf{n} \, dS$$

$$= -\oint_{\Sigma_{\mathrm{B}}} \exp(-in\varphi)(\mathbf{E} \times \hat{H}_{m,n}^- - \hat{E}_{m,n}^- \times \mathbf{H}) \cdot \mathbf{n} \, dS \qquad (10)$$

The left-hand side of eq 10 is the same as the integral in eq 8, and therefore finally eq 8 can be replaced by

$$c_{m,n}^+ = \frac{1}{N_{m,n}} \oint_{\Sigma_{\mathrm{B}}} \exp(-in\varphi)(\mathbf{E} \times \hat{H}_{m,n}^- - \hat{E}_{m,n}^- \times \mathbf{H}) \cdot (-\mathbf{n})$$

$$dS \qquad (11)$$

Equation 11 constitutes the main result of the present analysis, and it can be computed easily on a surface with a finite size (in
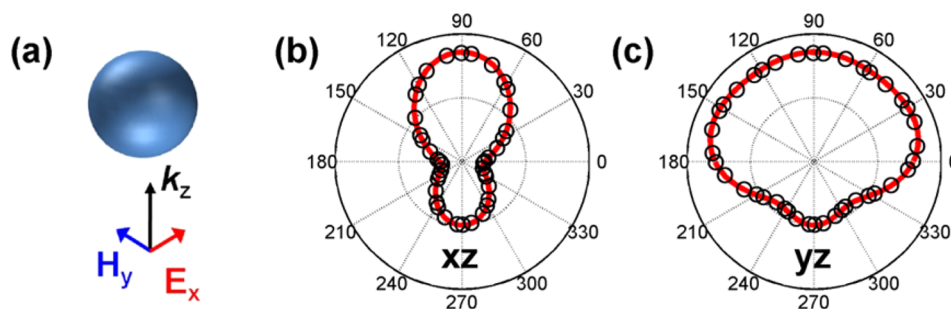
Figure 3. Plane wave scattering by a silicon (n = 3.5) nanosphere (radius R = 285 nm) in air at a wavelength of 1.5 μm. (a) The silicon sphere is illuminated by an x-polarized plane wave propagating along the $+z$ direction. (b and c) Radiation diagrams of the scattered field in the x−y plane and the y−z plane. Results obtained with the numerical tool and Mie theory are plotted with red curves and black circles.

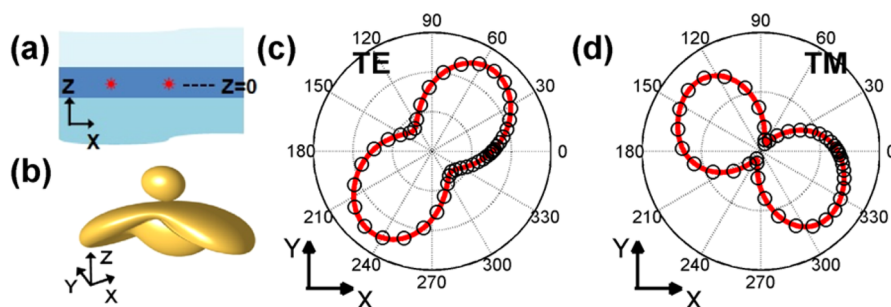**Figure 4.** Emission of two dipole sources inside a dielectric slab waveguide at a wavelength of 1 μm. (a) Sketch of the slab waveguide. The core layer (thickness 200 nm and refractive index 1.5) is surrounded by two semi-infinite media with indices 1 (above) and 1.2 (below). The dipole coordinates are (-100 nm, 0, 0) and (50 nm, 0, 0). (b) 3D free-space radiation diagram. The upper spherical (lower three-armed) part corresponds to radiation into the superstrate (substrate). (c and d) Radiation diagrams of TE_0 and TM_0 guided modes. Results obtained with the numerical toolbox and (semi)analytical calculation are shown with red curves and black circles, respectively.

contrast to eq 8). It implies that the amplitude of an outgoing mode can be formally computed by sending its associated ingoing mode into the stratified medium, as in the former section (i.e., the retrieval approach for free-space radiation diagram). We emphasize that the closed "box" Σ_B that fully encloses the local inhomogeneity has finite dimensions. Its surface normal **n** is directed inward; see Figure 2.

We remark that, because the r-dependent profiles are depicted by Hankel functions that diverge at $r = 0$, both $\Phi_{+m,n}$ and $\Phi_{-m,n}$ diverge at $r = 0$; however their sum $\Phi_{+m,n} + \Phi_{-m,n}$ remains finite. According to eq 7, one can easily find that in eqs 8 and 11 $\Phi_{-m,n}$ can be replaced by $\Phi_{+m,n} + \Phi_{-m,n}$, i.e., $c_{m,n}^+ = (\mathbf{E}, \mathbf{H}) \otimes (\Phi_{+m,n} + \Phi_{-m,n})$. We emphasize that this replacement, which is strictly rigorous from a mathematical standpoint, is crucial for numerical calculations (additional details can be found in the SI).

■ NUMERICAL TESTS

In this section, four examples are analyzed to show the capability of the open-source numerical toolbox based on the proposed retrieval approach. Additionally, the validity and accuracy of the numerical tool are tested in examples 1 and 2, for which the radiation diagrams retrieved by the numerical tool from the near-field obtained with COMSOL multiphysics are compared to diagrams obtained analytically. Examples 3 and 4 present two emblematic examples in the area of nanoantennas. Also, implementations of the examples 1 and 2 are provided in ref 25.

Example 1: Scattering by a Silicon Nanosphere in Free Space. We consider a silicon (n = 3.5) nanosphere of radius R = 285 nm placed in air and illuminated by an x-

polarized plane wave at a wavelength of 1.5 μm; see Figure 3a. The radiation diagram of the scattered field is calculated with COMSOL on a rectangular "box" that surrounds the nanosphere and with the present numerical toolbox. The results are displayed with the red curves in Figure 3b and c and are compared with radiation diagrams obtained with Mie theory[28] that are shown with black circles. The excellent agreement between the fully numerical approach and the analytical solution corroborates the accuracy of the numerical tool for retrieving the free-space radiation diagram.

Example 2: Emission of Two Dipole Sources in a Dielectric Slab Waveguide. In example 2, we consider a more intricate problem, in which two electric dipole sources are placed in a high-index dielectric slab waveguide (see Figure 4a) deposited on a substrate with a low refractive index. The polarizations of the two electric dipole sources are $J_1 = (\sqrt{2}/2, 0, \sqrt{2}/2)$ and $J_2 = (0, 1, 0)$, respectively. The dipoles are separated by 150 nm in the x direction. At the radiation wavelength of 1 μm, the waveguide supports only two modes, TE_0 (n_{eff} = 1.24) and TM_0 (n_{eff} = 1.20), with all higher order modes being cut off. The near-field distribution on a rectangular "box" that encloses the two sources is obtained with COMSOL and is used with the numerical toolbox to compute the free-space and guided-mode radiation diagrams. The results are shown in Figure 4b and 4c,d with red curves. As the refractive index of the substrate is larger than the one of the superstrate (air), light is dominantly radiated into the substrate. We additionally see that the radiation diagrams of TE and TM modes are very different. We have also calculated the radiation diagrams with an analytical expression for the field radiated by a dipole source in a stratified medium using Green's dyadics

approaches.[23,29,30] The results shown with black circles are in quantitative agreement with those obtained with the numerical toolbox. Similar agreement has been obtained for the free space radiation diagram (not shown). In addition, we have checked the energy conservation with a relative error of <1%, by comparing the total power radiated by the source doublet computed either directly by the total Poynting flux on a surface surrounding the doublet or indirectly from the radiation diagrams, summing over all free-space and guided modes.

The excellent agreement between the analytical calculations (black circles) and the fully numerical results (red curves) confirms the effectiveness of the present tool for treating guided modes of the stratified substrate.

Example 3: Scattering at a Metallic Hole. The launching of surface plasmon polaritons (SPPs) by metallic holes or slits has been widely studied in plasmonics.[15,16,18−20] In the third example, we consider the light scattering by a finite-depth rectangular metallic air hole etched in a semi-infinite metal substrate ($z < 0$) and illuminated by a normally incident plane wave; see the inset in Figure 5a. The hole creates a
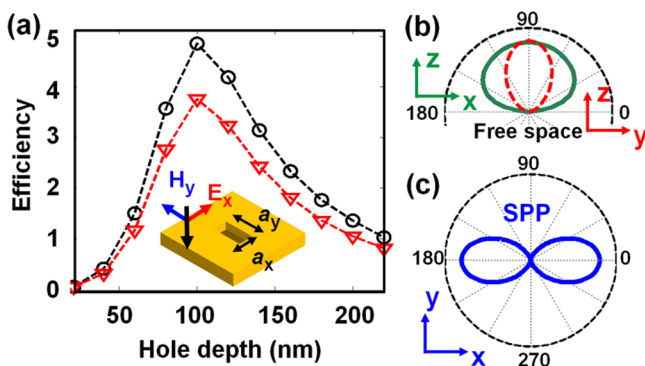

Figure 5. Scattering by a rectangular metallic hole etched in a metal substrate. (a) The hole is illuminated by an x-polarized plane wave at $\lambda_0 = 700$ nm impinging at normal incidence, as shown in the inset. Generation efficiencies of free-space scattered waves and SPPs as a function of hole depth are plotted as black circles and red triangles, respectively. (b) Free-space radiation diagram of the scattered wave in the $y−z$ plane (red dashed) and the $x−z$ plane (green solid). (c) SPP radiation diagram in the $x−y$ plane. The metal permittivity (gold) taken for the simulation is $\varepsilon_m = -15.83 + 1.28i$ at $\lambda_0 = 700$ nm.

backscattered field in free space and launches SPPs at the air−metal interface. With the present tool, we quantify the amount of backscattered waves and of launched SPPs. The size of the hole is fixed as $a_x = 100$ nm and $a_y = 400$ nm. We define the term *generation efficiency* as the ratio of the scattered power (of either free-space waves or SPPs) to the power incident over the hole area ($a_x \times a_y$). The efficiencies are displayed in Figure 5a, as a function of the hole depth.

For the present example, the scattered electromagnetic field on the "box" that encloses the hole is obtained using an aperiodic Fourier modal method.[31,32] Quantitative justification of the retrieved result by comparison with already known results is not made in this case, due to the lack of available solutions for the same problem in the literature. However, the response of subwavelength metallic holes can be approximately described as that of an effective magnetic dipole $\mathbf{m}_y$,[33] and this approximation shows good agreement with the free-space and SPP radiation diagrams shown in Figure 5b and c. The SPPs are

dominantly launched toward the x-direction, parallel to the incident polarization.

Example 4: Dipole Emission inside a Metal Patch Nanoantenna. Figure 6a−c depict a metal nanoantenna,
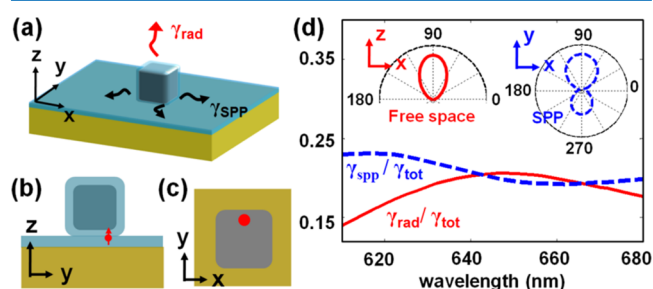

Figure 6. Dipole emission inside a metal nanoantenna. (a) 3D sketch of the nanoantenna. A silver nanocube ($65 \times 65 \times 65$ nm) with a 3 nm polymer coating is placed above a gold substrate covered by a 5 nm polymer (8 nm spacer in total). (b and c) Side and top views of the nanoantenna. A z-polarized electric dipole source shown with a red dot lies midway between the silver cube and gold substrate and is located near the edge of the cube. (d) Radiative ($\gamma_{rad}/\gamma_{tot}$) and plasmonic ($\gamma_{SPP}/\gamma_{tot}$) quantum-yield spectra. The top-left inset (red solid) shows the free-space radiation diagram in the $x−z$ plane at $\lambda_0 = 650$ nm. The top-right inset (blue dashed) shows the SPP radiation diagram in the horizontal $x−y$ plane at the same wavelength. In simulation, the refractive index of the polymer is 1.4; for the relative permittivities of silver and gold, a Drude model $\varepsilon_{Ag} = 1 - \omega_{Ag}^2/(\omega^2 - i\omega\Gamma_{Ag})$ and a Drude−Lorentz model $\varepsilon_{Au} = 8.1 - \omega_{Au}^2/(\omega^2 - i\omega\Gamma_{Au}) - 0.7\omega_L^2/(\omega^2 - \omega_L^2 - 2i\omega\Gamma_L)$ are adopted, with $\omega_{Ag} = 1.3 \times 10^{16}$ s^{-1}, $\Gamma_{Ag} = 1.6 \times 10^{14}$ s^{-1}, $\omega_{Au} = 1.3 \times 10^{16}$ s^{-1}, $\Gamma_{Au} = 4.13 \times 10^{13}$ s^{-1}, $\omega_L = 4.1 \times 10^{15}$ s^{-1}, and $\Gamma_L = 4.7 \times 10^{14}$ s^{-1}.

composed of a silver nanocube placed on a polymer film coated on a gold substrate and doped with a quantum emitter. Via the nanoantenna, the quantum emitter radiates into free space and launches SPPs on the dielectric−gold interface, with decay rates denoted by γ_{rad} and γ_{SPP}, respectively. We further denote by γ_{tot} the total decay rate. Nanocube antennas have been recently fabricated and tested, and extremely high Purcell factors and large radiative efficiencies have been reported.[10]

With COMSOL, we calculate the field radiated by the quantum emitter (modeled as a vertical electric dipole) on a box surrounding the nanocube and infer the radiation diagrams into the SPP and free-space modes. We also calculate the total power radiated by integrating the Poynting flux over a small box surrounding the dipole in the polymer layer. The SPP and free-space emission efficiencies are shown in Figure 6d. The computation is made over a spectral range covering the nanoantenna resonance at $\lambda_0 = 650$ nm. The radiation diagrams at λ_0 are shown in the insets. Note that at resonance, $\gamma_{rad}/\gamma_{tot}$ is about 20%. A larger value (∼50%) was predicted in ref 10, but we note that the authors in ref 10 are not equipped with the present numerical tool and that they infer γ_{rad} from the difference between the γ_{tot} and the nonradiative decay rate γ_{nrad} computed as the Joule loss inside the finite computational domain. Such an approach overestimates γ_{rad}, especially if SPPs that carry energy far away from the nanoantenna are efficiently launched, like in the present case. We believe that this highlights the importance of the present tool. Also, we remark that, as there is a fairly large portion of radiation that is directed into SPPs on the dielectric−metal interface, this type of device may be considered a good candidate for plasmon source.[6,34,35] A detailed study of the decay of quantum emitters in the

different decay channels (γ_{tot}, γ_{rad}, and γ_{SPP}) in such a device can be found in ref 36 as a function of the gap thickness, together with a thorough analysis of why quenching does not impose severe limitations on the quantum efficiency.

CONCLUSION

We have developed a general method for computing far-field free-space and guided-mode radiation diagrams of local inhomogeneities in stratified media. The far-field retrieval requires only the knowledge of the near-zone electromagnetic field (obtained by a Maxwell's equation solver) on a closed surface that envelops the local inhomogeneity. Moreover, the retrieval is based on rigorous mode decomposition. The accuracy of the tool has been corroborated by comparisons between fully numerical results and analytical results for two simple examples, and its range of applicability has been further illustrated with two examples taken from the recent literature on nanoplasmonics. Additionally, we have already successfully applied this numerical tool to various problems, including light extraction with optimized nanoparticles,[5] broadband absorbers,[37] and emission in metal nanogap structures[36] and metallic patch antennas.[38] Thus, we are confident that the tool can be widely used for various light emission and scattering problems in photonics and is compatible with virtually any Maxwell's equation solver.

Technical Remarks. This section briefly gathers some information on the usage of the numerical tool. (1) Retrieval procedure: To retrieve a free-space or guided-mode radiation diagram with the Matlab-based open-source software, beforehand one has to calculate the radiated or scattered electromagnetic field with any Maxwell's equation solver on a *rectangular* "box" that *fully* encloses the *local inhomogeneity*. Users have to set the refractive index and thickness of each layer (the online version handles nonmagnetic materials only). The numerical tool and its user guide are provided in ref 25. (2) Guided-mode radiation diagram: Waveguide-mode decomposition requires the profiles of the guided modes in the stratified media, which are found by a mode solver included in the open-source software. In addition, users should provide the modal effective index n_{eff} (potentially a c-number) and set the polarization of the desired mode. An accurate value of n_{eff} is not required, since it is computed precisely by the mode solver. Note that the n_{eff} of the cylindrical waveguide mode of a 3D stratified structure is the same as that of the 2D stratified structure (see SI). (3) CPU time: The open-source code is rather efficient. For instance, based on an ordinary workstation with a processor main frequency of 1.80 GHz, for the example 1 or 2 in this paper, the retrieval of the free-space radiation diagram (including both upper and lower free space) consumes about 100 s, and it costs just 2 s to compute the radiation diagrams of both the TE and TM modes for the example 2. CPU time is directly determined by the number of sample points on the "box" and the number of far-field directions that are computed.

ASSOCIATED CONTENT

ⓈSupporting Information

The Supporting Information is available free of charge on the ACS Publications website at DOI: 10.1021/acsphotonics.5b00559.

(1) Unconjugated form Lorentz reciprocity theorem. (2) Expressions of the cylindrical waveguide mode profiles.

(3) Mode orthogonality and normalization. (4) Removing the singularity of Hankel functions at $r = 0$. (5) Relation with the field equivalence principle (PDF)

AUTHOR INFORMATION

Corresponding Authors
*E-mail: jianji.yang.photonique@gmail.com.
*E-mail: jean-paul.hugonin@institutoptique.fr.
*E-mail: philippe.lalanne@institutoptique.fr.

Present Address
#Department of Electrical Engineering, Stanford University, Stanford, California 94305, United States.

Notes
The authors declare no competing financial interest.

REFERENCES

(1) Ferry, V. E.; Sweatlock, L. A.; Pacifici, D.; Atwater, H. A. Plasmonic nanostructure design for efficient light coupling into solar cells. *Nano Lett.* **2008**, *8*, 4391.

(2) Atwater, H. A.; Polman, A. Plasmonics for improved photovoltaic devices. *Nat. Mater.* **2010**, *9*, 205.

(3) Gu, X.; Qiu, T.; Zhang, W.; Chu, P. K. Light-emitting diodes enhanced by localized surface plasmon resonance. *Nanoscale Res. Lett.* **2011**, *6*, 199.

(4) Zhmakin, A. I. Enhancement of light extraction from light emitting diodes. *Phys. Rep.* **2011**, *498*, 189−241.

(5) Jouanin, A.; Hugonin, J.-P.; Besbes, M.; Lalanne, P. Improved light extraction with nano-particles offering directional radiation diagrams. *Appl. Phys. Lett.* **2014**, *104*, 021119.

(6) Liu, Y.; Palomba, S.; Park, Y.; Zentgraf, T.; Yin, X.; Zhang, X. Compact magnetic antennas for directional excitation of surface plasmons. *Nano Lett.* **2012**, *12*, 4853.

(7) Staude, I.; Miroshnichenko, A. E.; Decker, M.; Fofang, N. T.; Liu, S.; Gonzales, E.; Dominguez, J.; Luk, T. S.; Neshev, D. N.; Brener, I.; Kivshar, Y. Tailoring directional scattering through magnetic and electric resonances in subwavelength silicon nanodisks. *ACS Nano* **2013**, *7*, 7824.

(8) Coenen, T.; Arango, F. B.; Koenderink, A. F.; Polman, A. Directional emission from a single plasmonic scatterer. *Nat. Commun.* **2014**, *5*, 3250.

(9) Hancu, I. M.; Curto, A. G.; Castro-López, M.; Kuttge, M.; van Hulst, N. F. Multipolar interference for directed light emission. *Nano Lett.* **2014**, *14*, 166.

(10) Akselrod, G. M.; Argyropoulos, C.; Hoang, T. B.; Ciracì, C.; Fang, C.; Huang, J.; Smith, D. R.; Mikkelsen, M. H. Probing the mechanisms of large Purcell enhancement in plasmonic nanoantennas. *Nat. Photonics* **2014**, *8*, 835.

(11) Biagioni, P.; Huang, J. S.; Hecht, B. Nanoantennas for visible and infrared radiation. *Rep. Prog. Phys.* **2012**, *75*, 024402.

(12) Yu, N.; Genevet, P.; Kats, M. A.; Aieta, F.; Tetienne, J.-P.; Capasso, F.; Gaburro, Z. Light propagation with phase discontinuities: generalized laws of reflection and refraction. *Science* **2011**, *334*, 333−337.

(13) Lin, D.; Fan, P.; Hasman, E.; Brongersma, M. L. Dielectric gradient metasurface optical elements. *Science* **2014**, *345*, 298.

(14) Zheng, G.; Mühlenbernd, H.; Kenney, M.; Li, G.; Zentgraf, T.; Zhang, S. Metasurface holograms reaching 80% efficiency. *Nat. Nanotechnol.* **2015**, *10*, 308−312.

(15) Lalanne, P.; Hugonin, J. P.; Liu, H. T.; Wang, B. A microscopic view of the electromagnetic properties of subwavelength metallic surfaces. *Surf. Sci. Rep.* **2009**, *64*, 453−469.

(16) Liu, H.; Lalanne, P.; Yang, X. Y.; Hugonin, X. Y. Surface plasmon generation by subwavelength isolated objects. *IEEE J. Sel. Top. Quantum Electron.* **2008**, *14*, 1522−1529.

(17) Yao, W.; Liu, S.; Liao, H.; Li, Z.; Sun, C.; Chen, J.; Gong, Q. Efficient directional excitation of surface plasmons by a single-element nanoantennas. *Nano Lett.* **2015**, *15*, 3115.

(18) Kihm, H. W.; Koo, S. M.; Kim, Q. H.; Bao, K.; Kihm, J. E.; Bak, W. S.; Eah, S. H.; Lienau, C.; Kim, H.; Nordlander, P.; Halas, N. J.; Park, N. K.; Kim, D.-S. Bethe-hole polarization analyser for the magnetic vector of light. *Nat. Commun.* **2011**, *2*, 451.

(19) Rotenberg, N.; Spasenović, M.; Krijger, T. L.; le Feber, B.; García de Abajo, F. J.; Kuipers, L. Plasmon scattering from single subwavelength holes. *Phys. Rev. Lett.* **2012**, *108*, 127402.

(20) Coenen, T.; Polman, A. Optical properties of single plasmonic holes probed with local electron beam excitation. *ACS Nano* **2014**, *8*, 7350.

(21) Balanis, C. A. *Antenna Theory Analysis and Design*, 3rd ed.; Wiley-Interscience, 2005.

(22) Demarest, K.; Huang, Z.; Plumb, R. An FDTD near- to far-zone transformation for scatterers buried in stratified grounds. *IEEE Trans. Antennas Propag.* **1996**, *44*, 1150.

(23) Pors, A.; Bozhevolnyi, S. I. Quantum emitters near layered plasmonic nanostructures: decay rate contributions. *ACS Photonics* **2015**, *2*, 228.

(24) Zenneck, I. Propagation of plane electromagnetic waves along a plane conducting surface and its bearing on the theory of transmission in wireless telegraphy. *Ann. Phys.* **1907**, *23*, 846.

(25) The toolbox will soon be available at www.lp2n.institutoptique. fr/Membres-Services/Responsables-d-equipe/LALANNE-Philippe and can be obtained on request by then.

(26) Yeh, P. *Optical Waves in Layered Media*; J. Wiley and Sons: New York, 1988.

(27) Snyder, A. W.; Love, J. *Optical Waveguide Theory*; Springer: USA, 1983.

(28) Bohren, C. F.; Huffman, D. R. *Absorption and Scattering of Light by Small Particles*; Wiley, 1983.

(29) Sipe, J. E. New Green-function formalism for surface optics. *J. Opt. Soc. Am. B* **1987**, *4*, 481−489.

(30) Paulus, M.; Martin, O. J. F. Green's tensor technique for scattering in two-dimensional stratified media. *Phys. Rev. E: Stat. Phys., Plasmas, Fluids, Relat. Interdiscip. Top.* **2001**, *63*, 066615.

(31) Silberstein, E.; Lalanne, P.; Hugonin, J.-P.; Cao, Q. Use of grating theories in integrated optics. *J. Opt. Soc. Am. A* **2001**, *18*, 2865.

(32) Hugonin, J.-P.; Lalanne, J.-P. Perfectly matched layers as nonlinear coordinate transforms: a generalized formalism. *J. Opt. Soc. Am. A* **2005**, *22*, 1844.

(33) Jackson, J. D. *Classical Electrodynamics*; John Wiley & Sons Ltd., 1962.

(34) Falk, A. L.; Koppens, F. H. L.; Yu, C. L.; Kang, K.; de Leon Snapp, N.; Akimov, A. V.; Jo, M.-H.; Lukin, M. D.; Park, H. Near-field electrical detection of optical plasmons and single-plasmon sources. *Nat. Phys.* **2009**, *5*, 475−479.

(35) Gan, C. H.; Hugonin, J.-P.; Lalanne, P. Proposal for compact solid-state III-V single-plasmon sources. *Phys. Rev. X* **2012**, *2*, 021008.

(36) Faggiani, R.; Yang, J.; Lalanne, P. Quenching, plasmonic, and radiative decays in nanogap emitting devices. *ACS Photonics* **2015**, *2*, 1739.

(37) Langlais, M.; Hugonin, J.-P.; Besbes, M.; Ben-Abdallah, P. Cooperative electromagnetic interactions between nanoparticles for solar energy harvesting. *Opt. Express* **2014**, *22*, A577.

(38) Bigourdan, F.; Hugonin, J.-P.; Lalanne, P. Aperiodic-Fourier modal method for analysis of body-of-revolution photonic structures. *J. Opt. Soc. Am. A* **2014**, *31*, 1303.